AIP | Physics of Fluids

# Equilibrium electro-deformation of a surfactant-laden viscous drop

Herve Nganguia, Y.-N. Young, Petia M. Vlahovska, Jerzy Bławzdziewcz, J. Zhang et al.

Citation: Phys. Fluids **25**, 092106 (2013); doi: 10.1063/1.4821205
View online: http://dx.doi.org/10.1063/1.4821205
View Table of Contents: http://pof.aip.org/resource/1/PHFLE6/v25/i9
Published by the AIP Publishing LLC.

PHYSICS OF FLUIDS **25**, 092106 (2013)

# Equilibrium electro-deformation of a surfactant-laden viscous drop

Herve Nganguia,[1] Y.-N. Young,[1] Petia M. Vlahovska,[2] Jerzy Bławzdziewcz,[3] J. Zhang,[4] and H. Lin[4]
[1]*Department of Mathematical Sciences and Center for Applied Mathematics and Statistics, New Jersey Institute of Technology, Newark, New Jersey 07102, USA*
[2]*School of Engineering, Brown University, Providence, Rhode Island 02912, USA*
[3]*Department of Mechanical Engineering, Texas Tech University, Lubbock, Texas 79409, USA*
[4]*Department of Mechanical and Aerospace Engineering, Rutgers University, Piscataway, New Jersey 08854, USA*

(Received 28 February 2013; accepted 16 August 2013; published online 20 September 2013)

We theoretically investigate the deformation of a viscous drop covered with non-diffusing insoluble surfactant under a uniform DC electric field. At equilibrium, surfactant immobilizes the spheroidal drop surface and completely suppresses the fluid flow. In this work we focus on the equilibrium electro-deformation of a surfactant-laden drop in the leaky dielectric framework by developing (1) a second-order small-deformation analysis and (2) a spheroidal model for a highly deformed (prolate or oblate) drop. Both models are compared against experimental data and numerical simulation results in the literature. Our analysis shows how the existence of equilibrium spheroidal drop depends on the permittivity ratio, conductivity ratio, surfactant coverage, and the elasticity number. Furthermore, the spheroidal model highlights that differences between surfactant effects, such as tip stretching and surface dilution effects, are greatly amplified at large surfactant coverage and high electric capillary number. These surfactant effects are well captured in the spheroidal model, but cannot be described in the second-order small-deformation theory. © *2013 AIP Publishing LLC*. [http://dx.doi.org/10.1063/1.4821205]

## I. INTRODUCTION

Upon application of an electric field to a weakly conducting (leaky dielectric) drop suspended in another leaky dielectric fluid, free charges accumulate at the interface between the two fluids while the bulk remains electrically neutral.[1,2] Experiments show that a viscous drop can deform into a prolate (oblate) ellipsoid with the long axis aligned parallel (perpendicular) to the direction of the imposed electric field.[2–4] The flow circulation around the prolate drop is often opposite to that around the oblate drop, depending on the mismatch in electric conductivity, permittivity, and viscosity between the interior and exterior fluids. A brief and clear review of the droplet electrohydrodynamics (EHD) can be found in Ref. 5.

Taylor's spherical model[1] explains how different combinations of electric conductivity, permittivity, and fluid viscosity lead to either prolate or oblate shapes. For small to moderate electric field strengths, the balance between the surface tension, electric, and hydrodynamic stresses results in an equilibrium drop shape.[6–8] Small-deformation analysis provides good agreement with experiments for a slightly deformed viscous drop under a weak DC electric field.[1,9] When applied to large drop deformations under a strong electric field, however, small-deformation theories[1,9] give no quantitative agreement with experiments (see the Appendix).

Recently, Bentenitis and Krause[10] extended the leaky dielectric model for large electro-deformation of a non-charged viscous drop in a leaky dielectric fluid. Their large deformation analysis assumes spheroidal shapes and gives good agreement with most experiments for the prolate drops. Zhang *et al.*[11] refined the spheroidal model by projecting the stress balances onto the

 

corresponding (unsteady) velocity components, which is also done in the variational analysis[12] and reduced model analyses.[13,14] They obtained good agreement with experiments on prolate drops, but provided no comparison for the oblate drops in Ref. 11.

Under an even stronger electric field (beyond the critical strength), no steady equilibrium drop shape can be found and the drop keeps elongating until the eventual break-up into smaller droplets.[15–17] Conical points may form at the end of the viscous drop at high capillary number,[5] and small droplets may detach from the tip as a result of the tip-streaming instability.[18] The drop may also undergo undulation and break into several droplets of comparable sizes. The large deformation models[10,11] are inadequate to capture such extreme deformation, and numerical simulations have been conducted to investigate large electro-deformation in the framework of the leaky dielectric model.[5,8,19–24]

Tip-streaming has also been observed for a surfactant-covered drop in an extensional flow.[25–27] Surfactants (surface-active agents) are often used to facilitate deformation and breakup of fluid interface in many engineering applications,[26,28–30] and they are known to affect the stability of a viscous drop through a combination of reduced surface tension and the immobilizing (surface stiffening) effect of the Marangoni stress.[29,31–36]

The electro-deformation of a surfactant-laden viscous drop has been investigated by Ha and Yang[37,38] (experiments and small-deformation analysis) and later by Teigen and Munkejord[39] (axisymmetric numerical simulations). While Ha and Yang[37,38] concluded that surfactant enhances deformation for a prolate drop, Teigen and Munkejord[39] found that smaller deformation may be caused by diffusing surfactant for a prolate drop with a circulation from the pole to the equator (prolate B as categorized by Lac and Homsy[5]).

Two different modes of the drop breakup are observed in Ha and Yang's experiments[38] depending on the surfactant coverage. When the interface is clean or contaminated by a very small amount of surfactant, the drop bursts into several small droplets after forming bulbous ends. For a range of small surfactant concentration, tip-streaming is a prevalent drop breakup mode. If the surfactant concentration exceeds this range, the breakup mode goes back to the fragmentation with bulbous end formation. This indicates that, although not pronounced in the small-deformation limit, non-uniformity of the surfactant concentration is a decisive factor for the breakup mechanism of a prolate viscous drop in a DC field.

It is not clear how the two drop breakup modes are related to surfactant effects.[39,40] To investigate the origin of the two modes of breakup, we need to capture the large deformation of the surfactant-laden drop prior to breakup. In addition, a quantitative description of surfactant transport/redistribution is essential to accurately elucidate the surfactant effects. For example, how does surfactant alter the stability of an equilibrium drop shape? How does surfactant coverage affect the equilibrium drop deformation? How important is the Marangoni stress at different values of the electric capillary number?

To answer these questions, in this work we study the electro-deformation of a surfactant-laden viscous drop in the leaky dielectric EHD framework. We extend the approaches in Zhang *et al.*[11] to include the surfactant effects, and focus on how insoluble surfactant affects the existence of spheroidal drop and its deformation at equilibrium. Furthermore, we seek quantification of surfactant effects on a viscous drop under a DC electric field.

This paper is organized as follows. We formulate the problem in the leaky dielectric framework at the beginning of Sec. II. In Sec. II A we discuss the small-deformation analysis and present the equilibrium drop deformation at the second order. In Sec. II B we discuss the spheroidal model for large deformation and derive the equilibrium surface tension and the governing equation for the shape function. The validation of the spheroidal model without surfactant is given in the Appendix. In Sec. III we investigate surfactant effects on several aspects of a leaky dielectric viscous drop. We first examine how the existence of equilibrium spheroidal drop depends on various parameters in Sec. III A. We present comparison against experiments and numerical simulations of surfactant-covered drops in Sec. III B, where we further discuss the similarity and difference between prolate and oblate surfactant-covered drops in a DC electric field. In Sec. III C we elucidate the surfactant effects in terms of surface dilution and tip stretching, which can be quantified by the average surface tension. We show that our spheroidal model can capture both mechanisms as in direct numerical simulations,

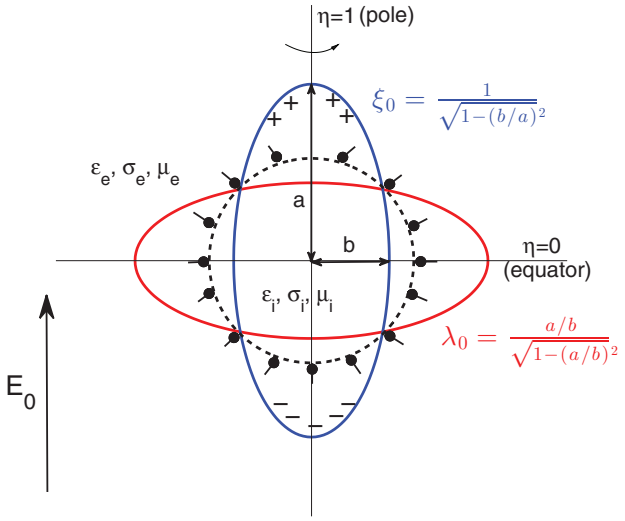


FIG. 1. Deformation of a viscous drop covered with insoluble surfactant (bead-rod particles) under a DC electric field $E_0\hat{\boldsymbol{z}}$. Starting from an initially spherical shape (dashed line), the drop can deform to either a prolate (labeled as $\xi_0$) or an oblate (labeled as $\lambda_0$) spheroid at equilibrium. $a$ and $b$ are distances from the center to the pole and equator, respectively.

while small-deformation theory cannot capture these effects. Finally, in Sec. IV we draw conclusion on our findings and discuss future research direction.

## II. PROBLEM FORMULATION

We consider a viscous leaky dielectric drop immersed in another leaky dielectric fluid as shown in Figure 1. Each fluid is characterized by the fluid viscosity $\mu$, dielectric permittivity $\varepsilon$, and conductivity $\sigma$ with the subscript denoting interior ($i$) or exterior ($e$) fluid. In this work the subscript "$r$" denotes the ratio between exterior and interior quantities: $\mu_r \equiv \mu_e/\mu_i$, $\varepsilon_r \equiv \varepsilon_e/\varepsilon_i$, and $\sigma_r \equiv \sigma_e/\sigma_i$. Typical leaky dielectric fluids are very viscous (for example the castor and silicone oils used by Ha and Yang[38] are hundreds or thousands times more viscous than water), and drops are of mm size. Hence the fluid flow in this system is in the creeping flow regime with negligible inertia, and the flow velocity in both interior and exterior fluids is therefore governed by the incompressible Stokes equations

$$\mu_j \nabla^2 \boldsymbol{u}_j = \nabla p_j, \quad \nabla \cdot \boldsymbol{u}_j = 0, \tag{1}$$

with $j = e$ or $j = i$. The boundary conditions for the velocity are $\boldsymbol{u} = 0$ in the far-field and $\boldsymbol{u} = \frac{d\boldsymbol{x}}{dt}$ on the drop surface, with $\boldsymbol{x}$ denoting the drop surface location.

The balance of stresses at the fluid interface gives

$$[\![\tau \cdot \boldsymbol{n}]\!] = \gamma (\nabla \cdot \boldsymbol{n}) \boldsymbol{n} - \nabla_s \gamma, \tag{2}$$

where $[\![f]\!] \equiv f_e - f_i$ denotes the difference between exterior ($e$) and interior ($i$), $\boldsymbol{n}$ is the unit normal vector on the drop surface, and $\nabla_s \equiv (\boldsymbol{I} - \boldsymbol{nn}) \cdot \nabla$ is the gradient projected on the drop surface. $\gamma$ is the surface tension that depends on the surfactant concentration $\Gamma$, and

$$\tau \equiv -p\mathbf{I} + \mu \left( (\nabla \boldsymbol{u})^T + \nabla \boldsymbol{u} \right) + \varepsilon \mathbf{E}\mathbf{E} - \frac{1}{2}\varepsilon (\mathbf{E} \cdot \mathbf{E}) \mathbf{I} = \mathbf{T} + \mathbf{S},$$

where $\mathbf{T} = -p\mathbf{I} + \mu \left( (\nabla \boldsymbol{u})^T + \nabla \boldsymbol{u} \right)$ is the hydrodynamic stress and $\mathbf{S} = \varepsilon \mathbf{E}\mathbf{E} - \frac{1}{2}\varepsilon (\mathbf{E} \cdot \mathbf{E}) \mathbf{I}$ is the Maxwell stress. The electric field is irrotational $\mathbf{E} = -\nabla\phi$, where $\phi$ is the electric potential that satisfies the Laplace equation both inside ($j = i$) and outside ($j = e$)

$$\nabla^2 \phi_j = 0. \tag{3}$$

In the far-field $\mathbf{E}$ is the imposed external electric field along the axis of symmetry: $-\nabla\phi_e = E_0\hat{\mathbf{z}}$. At the fluid interface the tangential electric field is continuous, while there is a jump in the normal electric field due to the balance of currents between the ohmic current and the rate of change of the surface charge density $q \equiv [\![-\varepsilon\nabla\phi\cdot\boldsymbol{n}]\!]$:

$$[\![-\nabla\phi\cdot\boldsymbol{t}]\!]=0, \quad [\![\sigma\nabla\phi\cdot\boldsymbol{n}]\!]=\frac{dq}{dt}=\frac{\partial q}{\partial t}+\nabla_s\cdot(\boldsymbol{u}_s q), \tag{4}$$

where $\boldsymbol{u}_s \equiv (\boldsymbol{I}-\boldsymbol{nn})\cdot\boldsymbol{u}$ is the tangential velocity on the surface.

The surfactant transport on the deforming drop surface is described by[41,42]

$$\frac{\partial\Gamma}{\partial t}+\nabla_s\cdot(\boldsymbol{u}_s\Gamma)+\kappa\boldsymbol{u}\cdot\boldsymbol{n}\Gamma = D_s\nabla_s^2\Gamma, \tag{5}$$

where $\Gamma$ is the surfactant concentration, $\kappa$ is the mean curvature of the surface, and $D_s$ is the surfactant diffusivity. In this work we focus on the non-diffusing limit and neglect the surface diffusion in Eq. (5). In our spheroidal model we use the Langmuir equation of state for surface tension of the surfactant-laden fluid interface:

$$\gamma = \gamma_0\left(1+E\ln\left(1-\frac{\Gamma}{\Gamma_\infty}\right)\right), \tag{6}$$

where $\gamma_0$ is the surface tension of a "clean" or surfactant-free drop, $\Gamma_\infty$ is the maximum packing concentration, and the elasticity number $E = RT\Gamma_\infty/\gamma_0$ quantifies the sensitivity of surface tension to changes in the surfactant concentration on the drop surface. $0.03 < E < 0.3$ is reasonable for low-molecular-weight surfactants[43] and polymeric surfactants.[44] For large $E$ the Marangoni stress alone cannot prevent the surface tension from going to zero[45] when the surfactant concentration is close to the critical micelle concentration $\Gamma_{\mathrm{CMC}}$, which happens during tip streaming[27,40,43,46] and thread formation.[47–50] Equation (6) no longer holds as $\Gamma \to \Gamma_{\mathrm{CMC}}$, and physics dictates that the surface tension plateaus to a minimum value for $\Gamma \geq \Gamma_{\mathrm{CMC}}$. A modified Langmuir equation of state has been adopted in Refs. 40 and 50: $\gamma = \max\left(\gamma_0\left(1+E\ln\left(1-\frac{\Gamma}{\Gamma_\infty}\right)\right), \gamma_{\min}\right)$. Value of $\gamma_{\min}$ varies for different combinations of fluid and surfactant. In this work we assume that $\gamma_{\min} = 0.1\gamma_0$ as this value has been reported under equilibrium conditions by DeBruijn.[25] In the following analyses and results the equilibrium surface tension $\gamma_{eq} \equiv \gamma_0(1+E\ln(1-\Gamma_{eq}/\Gamma_\infty)) = \gamma_0(1+E\ln(1-\chi))$ is used to scale surface tension and compute the electric capillary number, noting that $\chi$ is the normalized equilibrium surfactant coverage.

In the leaky dielectric hydrodynamics, $t_{c,j} \equiv \varepsilon_j/\sigma_j$ is an electric charging time, $t_{\gamma,j} \equiv \mu_j r_0/\gamma_0$ is a characteristic hydrodynamic time scale for a deformed drop to relax to its equilibrium shape, and often $t_{c,j} \ll t_{\gamma,j}$. A characteristic time scale in EHD is given by the inverse shear rate corresponding to the electric shear traction $t_{EHD} \equiv \mu_e/\varepsilon_e E_0^2$. In this work we focus on situations where $t_c \ll t_\gamma < t_{EHD}$. In the presence of surfactant we use the reduced surface tension $\gamma_{eq}$ to estimate the time $t_\gamma$. The ratio of the two time scales gives the electric capillary number $Ca_E \equiv t_{\gamma,e}/t_{EHD} = \frac{E_0^2 r_0\varepsilon_e}{\gamma_{eq}}$, which is also the ratio between characteristic electric stresses and surface tension.

### A. Second-order small-deformation analysis for a spherical drop

For small drop deformations, we seek a leading-order perturbative solution around a sphere in the form

$$\mathbf{E} = \mathbf{E}^\infty + \mathbf{E}^{(0)} + \cdots, \qquad \mathbf{u} = \mathbf{u}^{(0)} + \mathbf{u}^{(1)}(f,g) + \cdots. \tag{7}$$

The leading-order velocity field, $\mathbf{u}^{(0)}$, describes the flow about a spherical drop generated by the imposed electric field. This flow drives drop deformation and surfactant redistribution characterized by $f$ and $g$, respectively. For the electric field applied in the $z$-direction, the shape function $r_s$ and surfactant distribution are expressed as

$$r_s = r_0\left(1+f_{20}\left(-\tfrac{1}{3}+\cos^2\theta\right)\right), \ \Gamma = \Gamma_{\mathrm{eq}}\left(1+g_{20}\left(-\tfrac{1}{3}+\cos^2\theta\right)\right), \tag{8}$$

where $f_{20}$ and $g_{20}$ are the leading-order coefficients of scalar spherical harmonics (corresponding to $j = 2$ and $m = 0$ mode). The term $\mathbf{u}^{(1)}$ describes the flow driven by capillary and Marangoni stresses, i.e., relaxation of the deformed drop and surfactant back to the equilibrium spherical shape/uniform distribution.

In the small-deformation analysis both the drop deformation and the deviation of $\Gamma$ from the uniform distribution are assumed to be small,[51] therefore we use the linear equation of state for the surface tension

$$\gamma(\Gamma) = 1 + \tilde{E}\,(1 - \Gamma)\,, \tag{9}$$

where $\tilde{E} \equiv (\gamma_0 - \gamma_{eq})/\gamma_{eq}$. The relation between the capillary number based on the clean drop surface tension and the capillary number based on the equilibrium surface tension of the surfactant-covered drop is $Ca_0 = Ca_E \left(1 + \tilde{E}\right)^{-1}$, and the Marangoni number $Ma = \tilde{E} Ca_E^{-1}$.

The solution for $\mathbf{E}^{(0)}$ and $\mathbf{u}^{(0)}$ can be found in Refs. 52 and 53, and for $\mathbf{u}^{(1)}$ in Refs. 51 and 53. Combining these solutions we obtain the evolution equations for the shape and surfactant:

$$\frac{df_{20}}{dt} = c_{202} + Ca_0^{-1} C_c(\mu_r) f_{20} + Ma\left[C_{mf}(\mu_r) f_{20} + C_{mg}(\mu_r) g_{20}\right], \tag{10}$$

$$\frac{dg_{20}}{dt} = c_{222} + Ca_0^{-1} M_c(\mu_r) f_{20} + Ma\left[M_{mf}(\mu_r) f_{20} + M_{mg}(\mu_r) g_{20}\right]. \tag{11}$$

In the absence of surfactant, $Ma = 0$, the evolution equations reduce to the Taylor solution for a clean drop.

In Eqs. (10) and (11), the inhomogeneous term represents the distortion of the drop shape and surfactant distribution by the straining EHD flow:

$$c_{202} = \frac{9(5 + (6 + 5/\sigma_r)/\sigma_r + (5 + (9 + 5/\sigma_r)/\sigma_r - 19/\varepsilon_r)/\mu_r - 16/\varepsilon_r)}{(19/\mu_r + 16)(2/\mu_r + 3)(2 + 1/\sigma_r)^2}\,, \tag{12}$$

$$c_{222} = \frac{27((3 + (13 + 3/\sigma_r)/\sigma_r - 19/\varepsilon_r)/\mu_r + 2(1 + (6 + /\sigma_r)/\sigma_r - 8/\varepsilon_r)}{(19/\mu_r + 16)(2/\mu_r + 3)(2 + 1/\sigma_r)^2}\,. \tag{13}$$

The terms proportional to $Ca_0^{-1}$ describe relaxation of the drop shape and surfactant distribution driven by capillary (curvature) stresses:

$$C_c(\mu_r) = -\frac{40\mu_r(1 + \mu_r)}{(19 + 16\mu_r)(2 + 3\mu_r)}, \qquad M_c(\mu_r) = -\frac{24\mu_r(3 + 2\mu_r)}{(19 + 16\mu_r)(2 + 3\mu_r)}. \tag{14}$$

The terms proportional to $Ma$ describe relaxation of the drop shape and surfactant distribution driven by Marangoni stresses (surface tension gradients):

$$C_{mf}(\mu_r) = \frac{12\mu_r(3 + 2\mu_r)}{(19 + 16\mu_r)(2 + 3\mu_r)}\,, \qquad C_{mg}(\mu_r) = \frac{2\mu_r(1 + 4\mu_r)}{(19 + 16\mu_r)(2 + 3\mu_r)}\,, \tag{15}$$

$$M_{mf}(\mu_r) = \frac{6\mu_r(26 + 24\mu_r)}{(19 + 16\mu_r)(2 + 3\mu_r)}\,, \qquad M_{mg}(\mu_r) = -\frac{\mu_r(7 + 8\mu_r)}{(19 + 16\mu_r)(2 + 3\mu_r)}\,. \tag{16}$$

From Eqs. (10) and (11) we determine the discriminating function

$$D_L = \frac{9\left((1 + 1/\sigma_r)^2 - 4/\varepsilon_r\right)}{16(2 + 1/\sigma_r)^2}, \tag{17}$$

and $D_L = 0$ gives the boundary between prolate and oblate shapes on the $(\sigma_r, \varepsilon_r)$-plane (see Sec. III A). Continuing on to the second order terms (which we omit here) we obtain the equilibrium drop deformation $D_{eq} \equiv \frac{a-b}{a+b}$ ($a$ and $b$ are defined in Figure 1) as

$$D_{eq} = D_L Ca_E \left[1 + \frac{1/\sigma_r\,(1/\sigma_r(139/\sigma_r + 264) - 696/\varepsilon_r + 111) + 336/\varepsilon_r - 154}{80(1/\sigma_r + 2)^3} Ca_E\right]. \tag{18}$$

We remark that in the small deformation theory the equilibrium drop deformation $D_{eq}$ does not depend on $\mu_r$, and its dependence on $\tilde{E}$ is implicit through the equilibrium surface tension in the electric capillary number $Ca_E$.

### B. Large-deformation analysis for a spheroidal drop

For large spheroidal deformations, we seek a leading-order truncated solution in spheroidal coordinates. For a prolate spheroidal viscous drop we use the prolate spheroidal coordinates $(\xi, \eta)$ that are related to the cylindrical coordinates $(r, z)$ as

$$z = c\xi\eta, \quad r = \sqrt{x^2 + y^2} = c\sqrt{(\xi^2 - 1)(1 - \eta^2)}, \tag{19}$$

where $c \equiv \sqrt{a^2 - b^2}$ is the semi-focal length. Surfaces of constant $\xi \in [1, \infty)$ are spheroids while surfaces of constant $\eta \in [-1, 1]$ are hyperboloids. The drop surface is uniquely specified by $\xi_0 (= a/c)$ for a fixed drop volume. $a$ and $b$ are distances from center to pole and equator, respectively (see Figure 1), and can be expressed in terms of $\xi_0$ as $a(t) = r_0/\sqrt[3]{1 - \xi_0^{-2}}$ and $b(t) = r_0\sqrt[6]{1 - \xi_0^{-2}}$. In the following, $h_\xi$, $h_\eta$, and $h_\zeta$ denote the metric coefficients in the prolate spheroidal coordinates.

The axisymmetric two-dimensional incompressible flow is calculated from the stream function $\psi$ as $u_j = -\frac{1}{h_\xi h_\zeta}\frac{\partial \psi_j}{\partial \xi}$ and $v_j = \frac{1}{h_\eta h_\zeta}\frac{\partial \psi_j}{\partial \eta}$, where $u$ and $v$ are components of fluid velocity along $\boldsymbol{e}_\eta$ and $\boldsymbol{e}_\xi$, respectively. The stream function satisfies the equation

$$(\boldsymbol{E}^2)^2 \psi_j = 0, \text{ with } \boldsymbol{E}^2 = \frac{1}{c^2(\xi^2 - \eta^2)}\left[\left(\xi^2 - 1\right)\frac{\partial^2}{\partial \xi^2} + \left(1 - \eta^2\right)\frac{\partial^2}{\partial \eta^2}\right]. \tag{20}$$

The normal component of the interfacial velocity is

$$v(\xi_0) = \frac{d\boldsymbol{x}}{dt}\cdot\boldsymbol{e}_\xi = h_\xi\frac{d\xi_0}{dt} + \frac{d\boldsymbol{x}}{dc}\cdot\boldsymbol{e}_\xi\frac{dc}{dt} = \frac{r_0(1 - \xi_0^{-2})^{-5/6}}{3\xi_0^2}\frac{(1 - 3\eta^2)}{\sqrt{\xi_0^2 - \eta^2}}\frac{d\xi_0}{dt}, \tag{21}$$

while the tangential velocity has to be determined through the boundary conditions. The tangential and normal stress balances are given by

$$[\![\mathbf{T}_{\xi\eta}]\!] + [\![\mathbf{S}_{\xi\eta}]\!] + \nabla_s\gamma = [\![\mathbf{T}_{\xi\eta}]\!] + [\![\mathbf{S}_{\xi\eta}]\!] + \frac{1}{h_\eta}\frac{\partial\gamma}{\partial\eta} = 0, \tag{22}$$

$$[\![\mathbf{T}_{\xi\xi}]\!] + [\![\mathbf{S}_{\xi\xi}]\!] - \gamma\,(\nabla\cdot\boldsymbol{n}) = 0, \tag{23}$$

where

$$\mathbf{T}_{\xi\xi} = 2\mu\left(\frac{\partial v}{h_\xi\partial\xi} + \frac{u}{h_\xi h_\eta}\frac{\partial h_\xi}{\partial\eta}\right), \quad \mathbf{T}_{\xi\eta} = \mu\left(\frac{\partial(u/h_\eta)}{\partial\xi}\frac{h_\eta}{h_\xi} + \frac{\partial(v/h_\xi)}{\partial\eta}\frac{h_\xi}{h_\eta}\right), \tag{24}$$

$$\mathbf{S}_{\xi\xi} = \frac{\varepsilon}{2}\left(E_\xi^2 - E_\eta^2\right), \quad \mathbf{S}_{\xi\eta} = \varepsilon E_\xi E_\eta, \tag{25}$$

with $E_\xi \equiv -\frac{1}{h_\xi}\frac{\partial\phi}{\partial\xi}$ and $E_\eta \equiv -\frac{1}{h_\eta}\frac{\partial\phi}{\partial\eta}$ the normal and tangential electric fields, respectively. The electric potential $\phi$ is obtained by solving Eq. (3) for both $\phi_i$ and $\phi_e$ with boundary conditions on the interface:[11]

$$\phi_e = E_0 r_0\left(-\frac{c}{r_0}\xi_0 + \alpha(t)Q_1(\xi_0)\right)\eta, \quad \phi_i = E_0 r_0\beta(t)\xi_0\eta, \tag{26}$$

with $Q_1(\xi_0)$ the first-degree Legendre polynomial of the second kind. The coefficients $\alpha$ and $\beta$ are determined from Eq. (4). In this work we assume that the charging process on the drop surface is very fast ($t_c \ll t_{EHD}$) and neglect convection of surface charge:[54] $[\![\sigma\nabla\phi]\!] = \sigma_e\frac{\partial\phi_e}{\partial\xi} - \sigma_i\frac{\partial\phi_i}{\partial\xi} = 0$ at $\xi = \xi_0$. With this simplification, we obtain

$$\alpha(t) = \frac{c\xi_0\,(\sigma_r - 1)}{\xi_0\sigma_r Q_1' - Q_1}, \quad \beta(t) = \frac{c\sigma_r\left(Q_1 - \xi_0 Q_1'\right)}{\xi_0\sigma_r Q_1' - Q_1}, \tag{27}$$

for the prolate drop.

Using the method of semi-decomposition we express the general solution to Eq. (20) as

$$\psi = g_0(\xi)G_0(\eta) + g_1(\xi)G_1(\eta) + \sum_{n=2}^{\infty}\left(g_n(\xi)G_n(\eta) + h_n(\xi)H_n(\eta)\right), \tag{28}$$

where $G_n$ and $H_n$ are Gegenbauer functions of the first and second kind, respectively. $g_n$ and $h_n$ are linear combinations of $G_n$ and $H_n$. We refer interested readers to Dassios *et al.*[55] for detailed expressions of $G_n$, $H_n$, $g_n$, and $h_n$. Following Bentenitis and Krause[10] and Zhang *et al.*,[11] we seek a truncated solution

$$\psi_e = \left[A_3^1 H_1(\xi) + A_3^3 H_3(\xi)\right] G_3(\eta), \tag{29}$$

$$\psi_i = \left[B_3^3 G_3(\xi) + B_3^5 G_5(\xi)\right] G_3(\eta), \tag{30}$$

where coefficients $A_3^1$, $A_3^3$, $B_3^3$, and $B_5^3$ (functions of $\xi_0$, $\alpha$, and $\beta$) are determined from the boundary conditions.[10] At this order of truncation, the velocity continuity on the drop surface gives two equations. The other two equations have to be obtained from the stress balances in Eqs. (22) and (23), which can be projected onto the corresponding velocities (as done in the variational analysis[12]) to close the system:[11,14]

$$\int_{\xi=\xi_0(t)} u\left[[\![\mathbf{T}_{\xi\eta}]\!] + [\![\mathbf{S}_{\xi\eta}]\!] + \frac{1}{h_\eta}\frac{\partial\gamma}{\partial\eta}\right] ds = 0, \tag{31}$$

$$\int_{\xi=\xi_0(t)} v\left[[\![\mathbf{T}_{\xi\xi}]\!] + [\![\mathbf{S}_{\xi\xi}]\!] - \gamma\,(\nabla\cdot\boldsymbol{n})\right] ds = 0, \tag{32}$$

where the integrals are on the drop surface $\xi = \xi_0(t)$. For a clean drop $\gamma$ is constant, and the transient dynamics toward a unique equilibrium is well captured by the spheroidal model.[11] In the presence of non-diffusing surfactant, integrating the Marangoni stress in Eq. (31) leads to different equilibrium solutions as we vary the initial surfactant concentration distribution.

In our spheroidal model we take a different approach based on the fact that the fluid flow (and hence the viscous stress) vanishes at equilibrium for an axisymmetric drop covered with non-diffusing surfactant. Consequently, the tangential electric stress is balanced solely by the Marangoni stress

$$[\![\mathbf{S}_{\xi\eta}]\!] + \frac{1}{h_\eta}\frac{d\gamma}{d\eta} = 0. \tag{33}$$

To close the system we project the normal stress balance to the normal velocity

$$\int_{\xi=\xi_0(t)} v\left[[\![\mathbf{S}_{\xi\xi}]\!] - \gamma\,(\nabla\cdot\boldsymbol{n})\right] ds = 0. \tag{34}$$

Integrating Eq. (33) and scaling the electric potential by $E_0 r_0$, distance by $r_0$, and surface tension by $\gamma_{eq}$, we obtain the equilibrium (dimensionless) tension profile

$$\gamma = Ca_E f(\xi_0)\sqrt{\xi_0^2 - \eta^2} + A, \tag{35}$$

$$f(\xi_0) = \frac{\sqrt{\xi_0^2 - 1}}{c}\left[(-c + \alpha Q_1')(-c\xi_0 + \alpha Q_1) - \frac{\beta^2\xi_0}{\varepsilon_r}\right], \tag{36}$$

where the integration constant $A$ is determined from the conservation of total amount of surfactant. For the Langmuir equation of state (Eq. (6))

$$A = \frac{\gamma_0}{\gamma_{eq}}\left[1 - E - \ln\left(\frac{\int_{-1}^{1}\sqrt{\xi_0^2 - \eta^2}d\eta - \frac{2\chi}{c\sqrt{\xi_0^2-1}}}{\int_{-1}^{1}\sqrt{\xi_0^2 - \eta^2}e^{\frac{\gamma_{eq}}{\gamma_0}Ca_E f(\xi_0)\sqrt{\xi_0^2-\eta^2}}d\eta}\right)\right]. \tag{37}$$

Using Eq. (37) and the equilibrium surface tension from Eq. (35), the corresponding drop shape is obtained by solving for $\xi$ that satisfies Eq. (34), which upon substituting $v$, $\mathbf{S}_{\xi\xi}$, $\nabla \cdot \mathbf{n}$, and $\gamma$ into the integral and rearranging terms, is recast as

$$\frac{Ca_E}{c\xi_0}\left[(-c+\alpha Q_1')^2+\left(-c+\alpha\frac{Q_1}{\xi_0}\right)^2-2\beta^2\right]g(\xi_0)=\int_{-1}^{1}\frac{(1-3\eta^2)(2\xi_0^2-1-\eta^2)\gamma}{\sqrt{\xi_0^2-1}(\xi_0^2-\eta^2)^{3/2}}d\eta, \quad (38)$$

$$g(\xi_0)=\frac{\xi_0^2}{2}\int_{-1}^{1}\frac{(1-3\eta^2)(\eta^2-1)}{\xi_0^2-\eta^2}d\eta, \quad (39)$$

with $\alpha$ and $\beta$ given in Eq. (27). For a given $Ca_E$ and $(\sigma_r, \varepsilon_r)$, a solution $\xi_0$ of Eq. (38) is admissible if the corresponding tension and surfactant profiles are physical, i.e., tension is positive everywhere and the surfactant concentration never drops below zero.

For an oblate drop the derivation follows the above formulation with some modifications: The oblate spheroidal coordinates $(\lambda, \eta)$ are similarly expressed in the cylindrical coordinates $(r, z)$ as $z=\bar{c}\lambda\eta, r=\bar{c}\sqrt{(\lambda^2+1)(1-\eta^2)}$, with $\bar{c}\equiv\sqrt{b^2-a^2}$ for the oblate drop. Surfaces of constant $\lambda\in[0,\infty)$ are spheroids while surfaces of constant $\eta\in[-1,1]$ are hyperboloids. The oblate spheroidal coordinates can be transformed from the prolate spheroidal coordinates by substituting[55] $\xi\to\imath\lambda$ and $c\to-\imath\bar{c}$ with $\imath=\sqrt{-1}$. Similar transformation is also made in the derivation of the governing equations for the oblate case. For example, Eqs. (27) take the form

$$\alpha(t)=\frac{c\lambda_0(\sigma_r-1)}{\lambda_0\sigma_r Q_1'-Q_1}, \quad \beta(t)=-\imath\frac{c\sigma_r\left(Q_1-\lambda_0 Q_1'\right)}{\lambda_0\sigma_r Q_1'-Q_1}, \quad (40)$$

for the oblate drop. The stream function satisfies Eq. (20) with

$$\boldsymbol{E}^2=\frac{1}{\bar{c}^2(\lambda^2+\eta^2)}\left[\left(\lambda^2+1\right)\frac{\partial^2}{\partial\lambda^2}+\left(1-\eta^2\right)\frac{\partial^2}{\partial\eta^2}\right]. \quad (41)$$

## III. RESULTS

For a clean viscous drop, the spheroidal model can capture the equilibrium deformation up to $D_{eq}\approx 0.2$ for both prolate and oblate drops. In the Appendix we provide a detailed comparison between experiments,[6] numerical simulations,[5] and our implementation of the spheroidal model from Ref. 11 for both prolate and oblate clean drops. Consequently, we will focus on equilibrium drop deformation $|D_{eq}|\le 0.2$ in the following results and discussion. In addition, we fix the range of elasticity number $0.03\le E\le 0.3$ (for a detailed discussion on the realistic ranges of $E$ see Refs. 40 and 43). In the absence of surfactant, there are two prolate shapes: Prolate A with circulation from the equator to the pole, and prolate B with circulation from the pole to the equator (the same as in the oblate drop). As non-diffusing surfactant completely suppresses fluid flow at equilibrium (Figure 11), there is no distinction (in terms of flow around the drop) between the two prolate modes. The complete suppression of flow due to the Marangoni stress also implies that the equilibrium drop deformation does not depend on viscosity mismatch.

### A. Existence of spheroidal equilibrium

Taylor's spherical model for a clean viscous drop in a DC electric field[1] gives the boundary (dashed line in Figure 2(a) with $\mu_r=1$) between prolate and oblate drops in the $(\sigma_r, \varepsilon_r)$-plane. A prolate A drop is found for $\varepsilon_r>\sigma_r$ (above the dashed-dotted line), while a prolate B drop is found for $\varepsilon_r<\sigma_r$. More details on a clean viscous drop under a DC field can be found in Lac and Homsy.[5]

For a viscous drop covered with non-diffusing surfactant in a DC electric field, our second-order small-deformation predicts a spherical shape when $D_L=0$, which gives the solid lines in Figure 2(a). We cannot derive such a discriminating condition analytically in our spheroidal model, instead we numerically check the spheroidicity of the equilibrium shape around $D_L=0$ and we

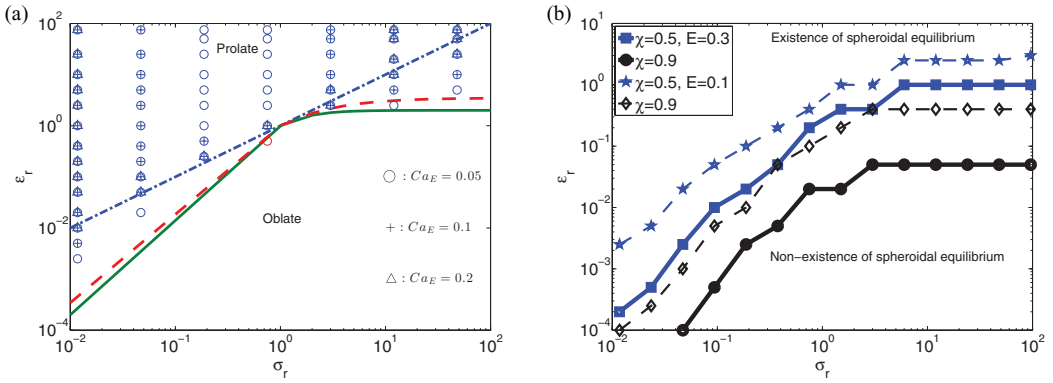


FIG. 2. Shape and equilibrium boundaries on the $(\sigma_r, \varepsilon_r)$-diagram. (a) Symbols denote that a spheroidal equilibrium can be found at those points with $(E, \chi) = (0.1, 0.1)$, $Ca_E = 0.05$, 0.1, and 0.2 (see legend). Solid line is the boundary between prolate and oblate drops from our small-deformation theory. (b) Boundaries for spheroidal equilibrium for $Ca_E = 0.2$ with different values of $E$ and $\chi$ (see legend). No spheroidal equilibrium is found below the boundary.

verify the transition between prolate and oblate across $D_L = 0$ boundary. In addition, our spheroidal model can provide the existence of admissible equilibrium spheroidal shapes in the $(\sigma_r, \varepsilon_r)$-plane. Using the Langmuir equation of state, we calculate the equilibrium surface tension and drop shape from Eqs. (35) and (38) for a given set of $(\sigma_r, \varepsilon_r)$. The existence of an equilibrium spheroidal drop is established if both the surface tension and surfactant distribution are physical: $\gamma > 0$ from Eq. (35) and $0 \leq \chi\Gamma < 1$ from the equation of state.

Figure 2(a) shows the existence of equilibrium for a spheroidal drop with $(E, \chi) = (0.1, 0.1)$ and three values of $Ca_E$ denoted by three types of symbols (see legend). Overall we observe that almost all (except one) equilibrium spheroidal solutions are prolate for $(E, \chi) = (0.1, 0.1)$, and the region of existence for spheroidal equilibrium gets smaller as $Ca_E$ increases. Figure 2(b) shows the boundaries for the existence of spheroidal equilibrium at $Ca_E = 0.2$ for four combinations of $E$ and $\chi$. For points on the boundaries, the value of $\varepsilon_r$ is the lower bound for a spheroidal equilibrium at that value of $\sigma_r$: No equilibrium can be found below this point. The lack of existence of a spheroidal equilibrium implies that the spheroidal shape is not stable for these parameters. It is possible that non-spheroidal axisymmetric equilibrium drop shape would be stable as in the case of clean drop.[5] We find a larger region of spheroidal equilibrium for larger $\chi$ and/or larger $E$.

### B. Comparison against experiments and numerical simulations

Ha and Yang[37,38] used soluble surfactant to investigate the electro-deformation of a surfactant-covered viscous drop under a DC electric field. The normalized surfactant coverage $\chi$ on the drop surface can be computed from the soluble surfactant concentration $C_\infty$ as $\chi = \frac{C_\infty}{C_\infty + \delta}$ if we assume that (1) surfactant exchange between the bulk and the drop surface is in equilibrium and (2) the soluble surfactant concentration is homogeneous and remains constant. The parameter $\delta$ is an equilibrium coefficient related to the adsorption/desorption rate coefficients.[26] We can estimate $E$ and $\delta$ by fitting the surface tension isotherm (Figure 9 of Ha and Yang[38]) to the formula

$$\gamma_C = \gamma_0 + RT\Gamma_\infty \ln\left(1 - \frac{C_\infty}{C_\infty + \delta}\right), \tag{42}$$

where $\gamma_C$ is the surface tension in the presence of soluble surfactant. We find that (1) for experiments 1–6, $E \approx 0.06$, $\delta \approx 6.46 \times 10^{-7} M$, and $0.13 < \chi < 0.99$, (2) for experiments 7–12, $E \approx 0.08$, $\delta \approx 6.00 \times 10^{-7} M$, and $0.14 < \chi < 0.99$, (3) for experiments 13–17, $E \approx 0.04$, $\delta \approx 7.74 \times 10^{-8} M$, and $0.5 < \chi < 0.99$, and (4) for experiments 18–21, $E \approx 0.04$, $\delta \approx 4.0 \times 10^{-5} M$, and $0.65 < \chi < 0.97$. Due to limited data points for experiments 18–21 (three points for fitting in Figure 9 of Ref. 38), the error of these estimates is quite large. There are no data for experiments 22–27 where the interior/exterior combination is silicone oil/castor oil, which is opposite to experiments 18–21.

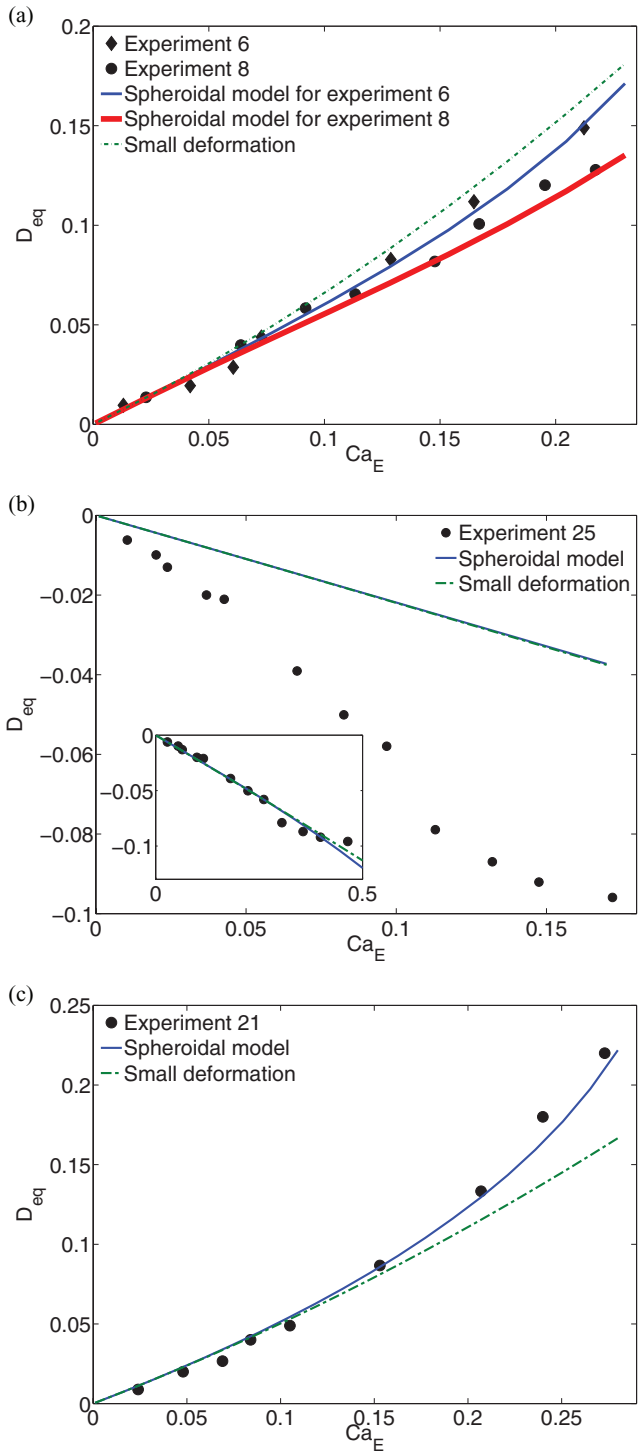


FIG. 3. Equilibrium deformation of a surfactant-laden drop from experiments[38] (symbols), second-order small-deformation results (dashed-dotted lines), and spheroidal results (solid lines). (a) Comparison for experiments 6 and 8 where $(\varepsilon_r, \sigma_r, \mu_r) = (0.0355, 10^{-6}, 10^3)$. $(E, \chi) = (0.06, 0.99)$ for experiment 6, and $(E, \chi) = (0.08, 0.999)$ for experiment 8. (b) Comparison for experiment 25 where $(\varepsilon_r, \sigma_r, \mu_r) = (1.3, 10, 15.38)$. $(E, \chi) = (0.04, 0.96)$ is used for the spheroidal model. In the inset we scale the capillary number from the experiments by 2.7, and find agreement with our modeling results. (c) Comparison for experiments 18–21 where $(\varepsilon_r, \sigma_r, \mu_r) = (0.73, 0.1, 12.5)$ and $(E, \chi) = (0.04, 0.96)$.

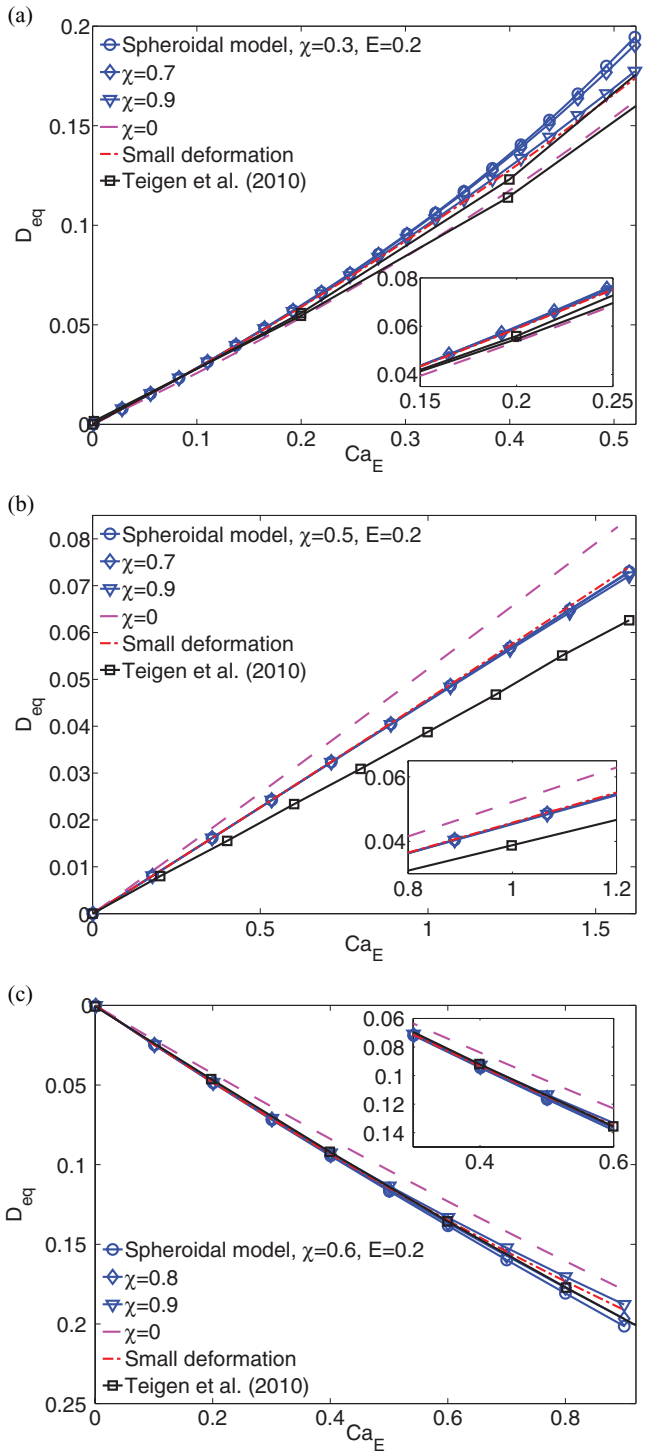


FIG. 4. Comparison of the equilibrium drop deformation computed numerically[39] (see legend), or analytically from our second-order small-deformation (dashed-dotted lines), and spheroidal theories (see legend). (a) Case A in Ref. 39 where $(\varepsilon_r, \sigma_r, \mu_r) = (1, 0.33, 1)$. (b) Case B in Ref. 39 where $(\varepsilon_r, \sigma_r, \mu_r) = (0.29, 0.33, 1)$. (c) Case C in Ref. 39 where $(\varepsilon_r, \sigma_r, \mu_r) = (0.5, 1, 1)$ .

We calculate the equilibrium drop deformation as a function of electric capillary number with the above estimates for ($E$, $\delta$) and $\chi$ at a given $C_\infty$. Figure 3 shows the comparison of $D_{eq}$ versus $Ca_E$ (or Weber number in Ha and Yang[38]) between experiments (symbols), second-order small-deformation (dashed-dotted line) and spheroidal model (solid line). Panel (a) is the comparison for a prolate drop (experiments 6 and 8 from Figure 4 of Ref. 38), and panel (b) is the comparison for an oblate drop (experiment 25 from Figure 6 of Ref. 38). We use experiment 25 to represent the data set of experiments 22–25. Because we cannot find any data to estimate ($E$, $\delta$) for experiments 22–25, we use the same value of ($E$, $\delta$) from experiment 21 (panel (c)), which is representative of experiments 18–21 (see Figure 5 of Ref. 38).

The equilibrium drop deformation from the small-deformation analysis is independent of ($E$, $\chi$), and agrees with the spheroidal model and the experiments for $Ca_E \leq 0.1$. The spheroidal model results, on the other hand, depend on ($E$, $\chi$) and agree well with the experiments for large $Ca_E$. From the prolate comparison in Figures 3(a) and 3(c), we conclude that the small-deformation results are reliable for $D_{eq}$ up to 0.1, while the spheroidal model agrees with the experimental data up to $D_{eq} \approx 0.2$. For the oblate deformation in Figure 3(b), small-deformation results agree well with spheroidal results, yet both are very different from the experimental data. Interestingly we find excellent agreement as shown in the inset of Figure 3(b) when we multiply the experimental capillary number by 2.7.

Teigen and Munkejord[39] numerically investigated the deformation of a viscous drop covered with diffusing insoluble surfactant with a small Peclet number (10). They studied three special cases: a prolate A drop, a prolate B drop, and an oblate drop. Their axisymmetric simulation results showed that the fluid flow at equilibrium is not completely suppressed by the diffusing surfactant. They also reported that surfactant increases the equilibrium drop deformation for prolate A and oblate drops, while for prolate B the deformation is reduced by surfactant.

Figure 4 shows the comparison of $D_{eq}$ for these three cases. For small $Ca_E$, we note that the spheroidal results agree with both the simulation results[39] and the small-deformation results in all three cases. This finding enhances the credibility of our oblate results in Figure 3(b), and implies that the oblate experimental data (experiments 22–25 and 27 from Figures 6 and 7 in Ref. 38) may be erroneous. Furthermore, we find that surfactant indeed increases $|D_{eq}|$ for small $Ca_E$. For large $Ca_E$, close inspection in Figure 4 shows a non-monotonic dependence on the surfactant coverage. We will explain such behavior in terms of surface dilution and tip stretching in Sec. III C.

Figure 5 shows the distribution of surfactant concentration and Marangoni stress and Figure 6 shows electric stresses and surface charge distribution for the parameters in Figure 4. Comparing Figure 5(a) with Figures 9 and 10 in Ref. 39 (arc length $s = 3$ in their results corresponds to $\eta = 0$), we observe similar surfactant concentration and Marangoni stress distributions, even though our Marangoni stress is quite insensitive to $\chi$. The electric stresses and induced surface charge in Figure 6 are also insensitive to $\chi$. We further note that, even though the non-diffusing surfactant completely suppresses the fluid flow, our spheroidal results for the prolate B parameters (Case B) are more similar to results for the oblate parameters (Case C) in terms of distributions of Marangoni stress, tangential electric stress and the induced surface charge.

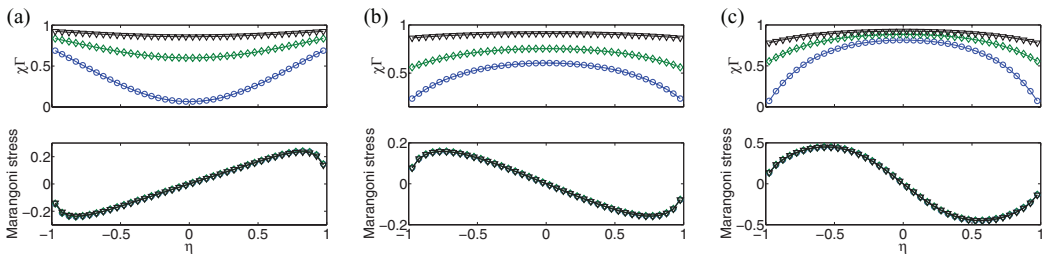


FIG. 5. Distribution of surfactant concentration $\chi\Gamma$ and Marangoni stress for Figure 4. (a) Case A in Ref. 39 with $Ca_E = 0.46$. (b) Case B in Ref. 39 with $Ca_E = 1.6$. (c) Case C in Ref. 39 with $Ca_E = 0.9$.

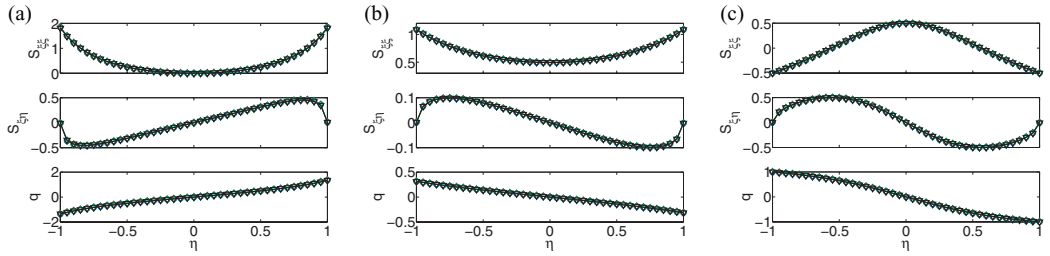


FIG. 6. Distribution of normal electric stress $S_{\xi\xi}$, tangential electric stress $S_{\xi\eta}$, and surface charge $q$ for Figure 4. (a) Case A in Ref. 39 with $Ca_E = 0.46$. (b) Case B in Ref. 39 with $Ca_E = 1.6$. (c) Case C in Ref. 39 with $Ca_E = 0.9$.

### C. Surface dilution versus tip stretching

A measure to quantify the surfactant effect is the average surface tension defined as[40]

$$\gamma_{\text{avg}} \equiv \frac{\int_{\xi=\xi_0(t)} \gamma\, ds}{\int_{\xi=\xi_0(t)} ds}. \tag{43}$$

At high surfactant coverage, drop deformation dilutes the surfactant concentration and increases the average surface tension $\gamma_{\text{avg}} > 1$, leading to smaller drop deformation than the uniform tension (clean drop) case at a given $Ca_E$. On the other hand, if the surfactant coverage is small, larger surfactant concentration gradient is easily realized when surfactant accumulates at the drop tips, leading to higher curvature by stretching out to the exterior (and hence larger drop deformation).[40] The latter mechanism is called tip stretching for $\gamma_{\text{avg}} < 1$, while the former mechanism is called surface dilution for $\gamma_{\text{avg}} > 1$.

Adding more surfactant in the tip-stretching dominant regime leads to larger drop deformation.[40,43] Another signature of tip stretching is the large surfactant concentration gradient, and hence the Marangoni stress. However, when surface dilution takes over, more surfactant leads to less drop deformation and smaller surfactant concentration gradient (Marangoni stress) is expected.[40]

Figure 7 shows the average surface tension for the three cases in Figure 4. As the surfactant coverage increases we see that the dominant mechanism transitions from tip stretching to surface dilution in all three cases. Significant decrease in drop deformation with increasing surfactant coverage is observed for both prolate A (Case A, Figure 4(a)) and oblate (Case C, Figure 4(c)), while very little change in $D_{eq}$ is found for prolate B.

To further illustrate that the average surface tension is a good indicator for the underlying physical mechanisms involving surfactant, we compute the equilibrium drop shape using the same parameters for Figure 19 in Lac and Homsy[5] with different values of surfactant coverage $\chi$. Figure 8(a) shows $D_{eq}$ versus $Ca_E$ at four values of surfactant coverage, and Figure 8(b) shows the corresponding equilibrium surfactant concentration distribution (top) and Marangoni stress (bottom). We find that surfactant-laden drop has larger $D_{eq}$ for $0 < \chi \leq 0.7$. For $\chi = 0.9$ the large surfactant coverage leads to smaller $D_{eq}$ compared to the clean drop for $Ca_E > 0.03$. The Marangoni stress distribution

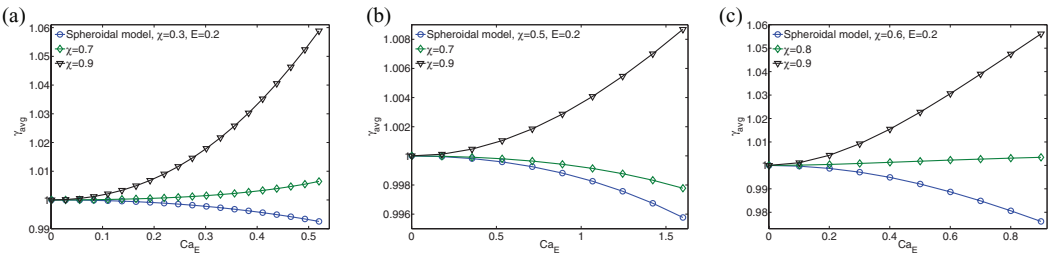


FIG. 7. Average surface tension for the three cases in Ref. 39. Panels (a), (b), and (c) correspond to Cases A, B, and C, respectively.

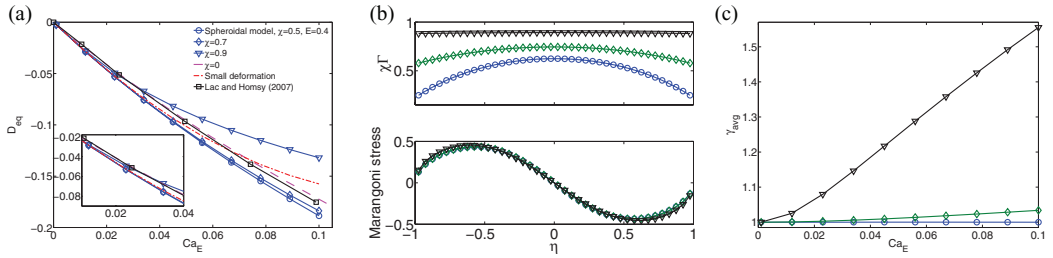


FIG. 8. Surfactant effects on drop deformation for $(\varepsilon_r, \sigma_r, \mu_r) = (0.05, 0.5, 1)$, where an equilibrium oblate clean drop is found for all values of $Ca_E$.[5] (a) $D_{eq}$ versus $Ca_E$ at different $\chi$. (b) Surfactant concentration $\chi\Gamma$ (top) and Marangoni stress (bottom). (c) $\gamma_{\text{avg}}$ versus $Ca_E$.

(panel (b)) is almost identical for all surfactant coverages, while the average surface tension in panel (c) clearly indicates that surface dilution is much more dominant at $\chi = 0.9$, and thus smaller drop deformation for $\chi = 0.9$ in panel (a). Similar behavior is also reported for the surfactant effects on the deformation of a viscous drop in an extensional flow.[40,43] Such non-monotonic surfactant dependence of the equilibrium drop deformation is not captured by the second-order small-deformation theory.

## IV. SUMMARY

In this work we investigate theoretically the effect of surfactant on equilibrium drop deformation. Small deviations from sphericity are analyzed by a second-order small-deformation theory. Large deformations are described by a spheroidal model based on Ref. 11. In contrast to the approach in Ref. 11, the tangential electric stress is balanced by the Marangoni stress at equilibrium in the presence of non-diffusing surfactant. As a result the equilibrium surface tension is obtained from the tangential electric stress, and we numerically solve for the corresponding equilibrium shape for a given equation of state. We determine the range of validity of both spheroidal model and the small-deformation model by comparing against experiments[38] and numerical simulations,[39] using exactly the same values for physical parameters. For small $Ca_E$ we always find perfect agreement between small-deformation results and spheroidal results. Between the two models and experiments, we find that our spheroidal model gives better agreement with the experiments over a wider range of $Ca_E$. Comparison with numerical simulations for Case A in Ref. 39 shows quantitative agreement in the distribution of surfactant concentration and Marangoni stress.

As non-diffusing surfactant suppresses the fluid flow by immobilizing the interface via the Marangoni stress at equilibrium, adding non-diffusing surfactant eliminates the distinction between prolate A and prolate B drops in terms of fluid flow around the viscous drop. However we still observe different features of tangential electric stress and surface charge distribution between these two parameter regimes in the presence of surfactant: For parameters in the prolate B clean drop regime, the Marangoni stress, tangential electric stress $S_{\xi\eta}$ and surface charge $q$ are similar to those in the oblate clean drop regime. To our knowledge this has not been reported in the literature.

Furthermore, our spheroidal model captures the surfactant effects at large electric capillary number. In the tip stretching regime the drop deformation is increased by a small amount of surfactant while in the surface dilution regime the drop deformation is decreased by increasing surfactant coverage. We find more pronounced surface dilution effect at large $Ca_E$. We also investigate how the existence of an equilibrium spheroidal shape depends on the electric capillary number, elasticity number, and the surfactant coverage. At low surfactant coverage we find equilibrium mostly for prolate shape, and increasing the electric capillary number diminishes the existence of equilibrium shape. At high surfactant coverage surface dilution takes over and stabilizes the equilibrium spheroidal drop at high $Ca_E$.

It will be interesting to see how surfactant diffusion and solubility may modify equilibrium results reported in this work. In our time-dependent calculations we find that, in some cases, non-diffusing surfactant cannot immobilize the drop surface to prevent the surfactant concentration from reaching the maximum packing. In reality surfactant diffusion is a weak effect, and is unlikely to

greatly change our conclusion on the spheroidal equilibrium. However, the lack of a spheroidal equilibrium may be an indication that a non-spheroidal equilibrium shape is favored instead. We are now using an axisymmetric numerical code to investigate how the surfactant distribution and circulation may contribute to non-spheroidal drop deformation and different modes of drop breakup.

## ACKNOWLEDGMENTS

H.N. and Y.N.Y. acknowledge partial support from NSF Grant Nos. DMS-1009105 and DMS-1222550. P.M.V. acknowledges partial support from NSF Grant No. CBET-1132614. J.Z. and H.L. acknowledge support from NSF Grant No. CBET-0747886.

## APPENDIX: MODEL VALIDATION: CLEAN SPHEROIDAL DROP

The electro-deformation of a clean viscous drop under a DC electric field has been investigated analytically,[1,9–11,56] numerically,[5,21,54] and experimentally.[1,6,15,57] In particular, large electro-deformation has been modeled analytically in Bentenitis and Krause[10] and Zhang *et al.*[11] Their theoretical results compare reasonably well with experimental data, though the agreement is better

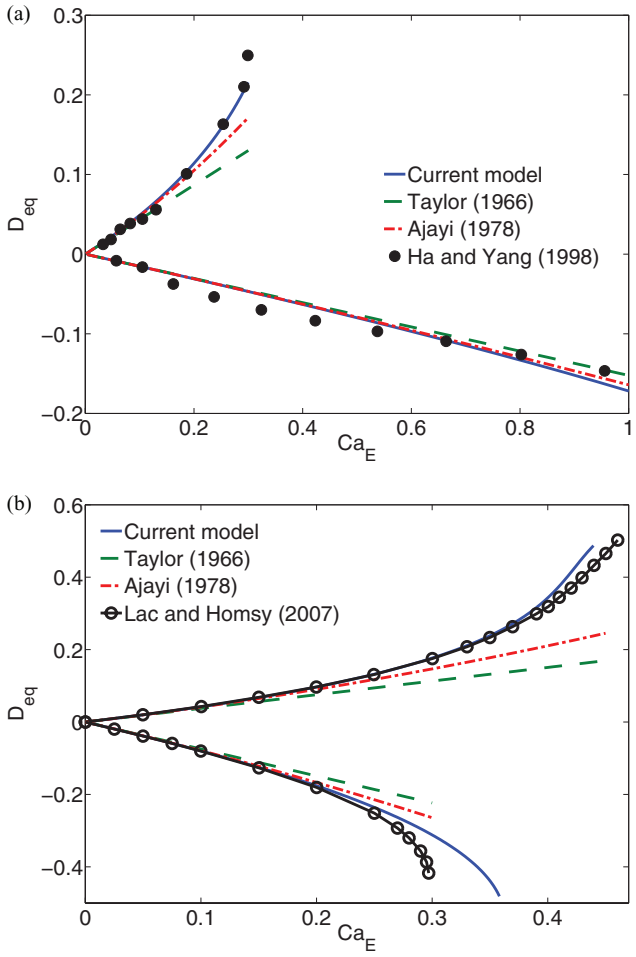


FIG. 9. Equilibrium deformation for a clean drop in a DC electric field: Comparison between the spheroidal model[11] (solid line), Taylor's spherical model[1] (dashed line), and Ajayi's second-order model[9] (dashed-dotted line). (a) Symbols are experimental results from Ref. 6 where $(\varepsilon_r, \sigma_r, \mu_r) = (0.73, 0.1, 1.14)$ for the prolate drop ($D_{eq} > 0$), $(\varepsilon_r, \sigma_r, \mu_r) = (1.39, 6.67, 1.28)$ for the oblate drop ($D_{eq} < 0$). (b) Symbols are numerical results from Ref. 5 where $(\varepsilon_r, \sigma_r, \mu_r) = (0.02, 0.04, 1)$ for the prolate drop ($D_{eq} > 0$), and $(\varepsilon_r, \sigma_r, \mu_r) = (0.5, 10, 1)$ for the oblate drop ($D_{eq} < 0$).

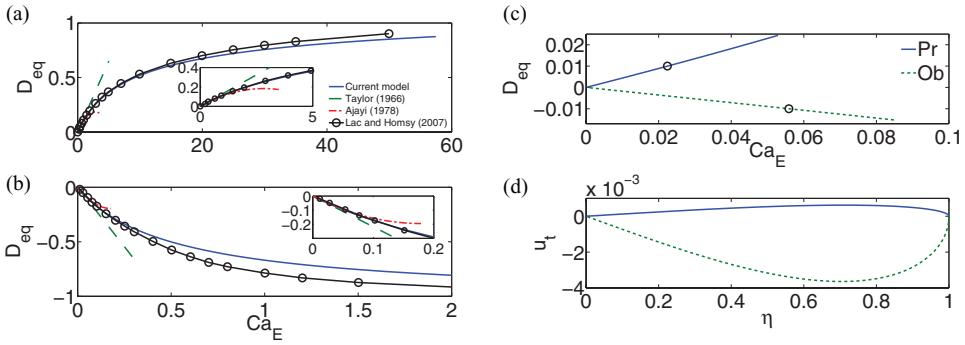


FIG. 10. ((a) and (b)) Comparison of the current model (solid line), Taylor's spherical model[1] (dashed line), and Ajayi's second order approximation[9] (dashed-dotted line). Symbols are numerical results from Ref. 5. $(\varepsilon_r, \sigma_r, \mu_r) = (25, 10, 1)$ for panel (a) and $(\varepsilon_r, \sigma_r, \mu_r) = (0.05, 0.5, 1)$ for panel (b). ((c) and (d)) Comparison of the tangential flow between an oblate $(\varepsilon_r, \sigma_r, \mu_r) = (1.37, 10, 1)$ and a prolate $(\varepsilon_r, \sigma_r, \mu_r) = (0.73, 0.1, 1)$ drop at deformation $|D_{eq}| = 0.01$.

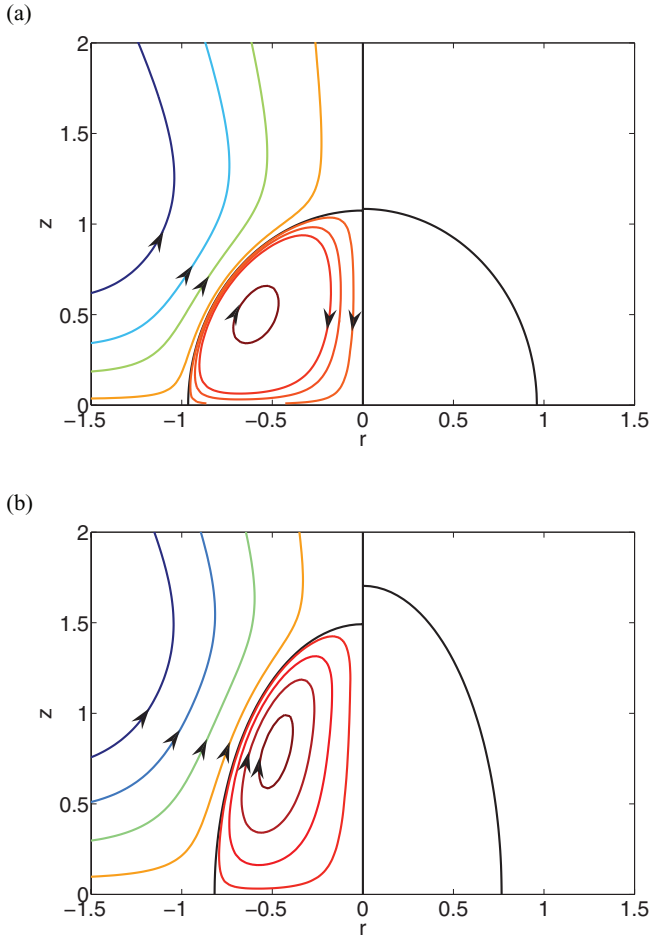


FIG. 11. Comparison of equilibrium drop shape and circulation for Case A in Ref. 39 where $(\varepsilon_r, \sigma_r, \mu_r) = (1, 0.33, 1)$. $Ca_E$=0.2 for panel (a) and $Ca_E = 0.8$ for panel (b). Clean drop with circulation is on the left of each panel. On the right the drop is covered with $\chi = 0.7$ and the circulation is completely suppressed by the non-diffusing surfactant.

for the prolate cases than for the oblate cases in Ref. 10, and no results for the oblate case in Ref. 11. As a validation Y.N.Y. and H.N. implemented their own spheroidal model for both prolate and oblate spheroidal shapes, and compared theoretical predictions against experimental and numerical data for a clean viscous drop.

Figure 9 shows the dependence of equilibrium drop deformation on the electric capillary number $Ca_E$ predicted by three models. The theory is compared to experimental data (Figure 9(a)) and numerical simulation data (Figure 9(b)). Results from the present spheroidal model (solid curve) agree with both experimental data and the numerical simulations for a wide range of electric capillary number. In addition, we also note that the spheroidal model is almost exactly the same as the numerical simulation results for deformation $|D_{eq}|$ up to 0.2. Taylor's prediction gives reasonable agreement for $Ca_E$ up to 0.1 for most cases, while Ajayi's second-order approximation is consistently between Taylor's results and the spheroidal results for all four cases in Figure 9.

Figure 10(a) shows two more examples of comparison of equilibrium drop deformation between models and results from the boundary integral simulations of Lac and Homsy[5] with parameters that allow an equilibrium spheroidal drop for all values of the capillary number for both prolate (panel (a)) and oblate (panel (b)) drops. For the prolate case we see that the spheroidal model is far more superior than Taylor's or Ajayi's results, and good agreement is obtained for deformation up to $D_{eq} \approx 0.5$. For the oblate case the spheroidal model gives the best agreement again, yet it begins to deviate significantly from the axial-symmetric results around $|D_{eq}| > \approx 0.3$. Figures 10(c) and 10(d) show a comparison of tangential flow between prolate and oblate. At a given $Ca_E$ the prolate deformation is larger than the oblate deformation. For a given deformation, say $D_{eq} = 0.01$ (circles in Figure 10(c)), the fluid flow is larger for the prolate drop than for the oblate drop. Based on these findings we conclude that an initially uniform surfactant concentration will be much more redistributed in the oblate case before an equilibrium is reached and the Marangoni stress is established.

Finally, Figure 11 shows the comparison of equilibrium drop shape and circulation between clean and surfactant-covered drops from our spheroidal model with $\chi = 0.7$ and parameters for Case A in Ref. 39. On the left is a clean drop with circulation, and on the right is a surfactant-covered drop at equilibrium, depleted of any flow due to the immobilized fluid interface covered with non-diffusing surfactant.

[1] G. Taylor, "Studies in electrohydrodynamics. I. The circulation produced in a drop by electric field," Proc. R. Soc. London, Ser. A **291**, 159–166 (1966).
[2] J. R. Melcher and G. I. Taylor, "Electrohydrodynamics: A review of the role of interfacial shear stresses," Annu. Rev. Fluid Mech. **1**, 111–146 (1969).
[3] R. S. Allan and S. G. Mason, "Particle behaviour in shear and electric fields. I. Deformation and burst of fluid drops," Proc. R. Soc. London, Ser. A **267**, 45–61 (1962).
[4] D. A. Saville, "Electrohydrodynamics: The Taylor-Melcher leaky dielectric model," Annu. Rev. Fluid Mech. **29**, 27–64 (1997).
[5] E. Lac and G. M. Homsy, "Axisymmetric deformation and stability of a viscous drop in a steady electric field," J. Fluid Mech. **590**, 239–264 (2007).
[6] J.-W. Ha and S.-M. Yang, "Deformation and breakup of Newtonian and non-Newtonian conducting drops in an electric field," J. Fluid Mech. **405**, 131–156 (2000).
[7] E. K. Zholkovskij, J. H. Masliyah, and J. Czarnecki, "An electrokinetic model of drop deformation in an electric field," J. Fluid Mech. **472**, 1–27 (2002).
[8] G. Supeene, C. R. Koch, and S. Bhattacharjee, "Deformation of a droplet in an electric field: Nonlinear transient response in perfect and leaky dielectric media," J. Colloid Interface Sci. **318**, 463–476 (2008).
[9] O. O. Ajayi, "A note on Taylor's electrohydrodynamic theory," Proc. R. Soc. London, Ser. A **364**, 499–507 (1978).
[10] N. Bentenitis and S. Krause, "Droplet deformation in DC electric fields: The extended leaky dielectric model," Langmuir **21**, 6194–6209 (2005).
[11] J. Zhang, J. Zahn, and H. Lin, "Transient solution for droplet deformation under electric fields," Phys. Rev. E **87**, 043008 (2013).
[12] S. Chandrasekhar, *Hydrodynamic and Hydromagnetic Stability* (Dover Publications, Inc., New York, 1981), pp. 124–126.
[13] J. D. Sherwood, "Breakup of fluid droplets in electric and magnetic fields," J. Fluid Mech. **188**, 133–146 (1998).
[14] N. Dubash and A. J. Mestel, "Behavior of a conducting drop in a highly viscous fluid subject to an electric field," J. Fluid Mech. **581**, 469–493 (2007).
[15] J.-W. Ha and S.-M. Yang, "Electrohydrodynamics and electrorotation of a drop with fluid less conducting than that of the ambient fluid," Phys. Fluids **12**, 764 (2000).
[16] R. T. Collins, J. J. Jones, M. T. Harris, and O. A. Basaran, "Electrohydrodynamic tip streaming and emission of charged drops from liquid cones," Nat. Phys. **4**, 149–154 (2008).

[17] R. T. Collins, K. Sambath, M. T. Harris, and O. A. Basaran, "Scaling laws for the disintegration of electrified drops," Proc. Natl. Acad. Sci. U.S.A. **110**, 4905–4910 (2013).
[18] G. I. Taylor, "Conical free surfaces and fluid interfaces," in *Proceedings of the 11th International Congress of Theoretical and Applied Mechanics (Munich 1964)* (Springer Verlag, Heidelberg, 1964), pp. 790–796.
[19] P. R. Brazier-Smith, "Stability and shape of isolated and pairs of water drops in an electric field," Phys. Fluids **14**, 1 (1971).
[20] P. R. Brazier-Smith, S. G. Jennings, and J. Latham, "An investigation of the behaviour of drops and drop-pairs subjected to strong electric forces," Proc. R. Soc. London, Ser. A **325**, 363–376 (1971).
[21] M. Miksis, "Shape of a drop in an electric field," Phys. Fluids **24**, 1967 (1981).
[22] O. A. Basaran and L. E. Scriven, "Axisymmetric shapes and stability of charged drops in an external electric field," Phys. Fluids **1**, 799 (1989).
[23] R. Suryo and O. A. Basaran, "Tip streaming from a lipid drop forming from a tue in a co-flowing outer fluid," Phys. Fluids **18**, 082102 (2006).
[24] C. Zhou, P. Yue, and J. J. Feng, "Formation of simple and compound drops in microfluidic devices," Phys. Fluids **18**, 092105 (2006).
[25] R. A. DeBruijn, "Tipstreaming of drops in simple shear flows," Chem. Eng. Sci. **48**, 277–284 (1993).
[26] S. L. Anna and H. C. Mayer, "Microscale tipstreaming in a microfluidic flow focusing device," Phys. Fluids **18**, 121512 (2006).
[27] M. R. Booty and M. Siegel, "Steady deformation and tip-streaming of a slender bubble with surfactant in extensional flow," J. Fluid Mech. **544**, 243–275 (2005).
[28] P. K. Notz, A. U. Chen, and O. A. Basaran, "Satellite drops: Unexpected dynamics and change of scaling during pinch-off," Phys. Fluids **13**, 549–552 (2001).
[29] F. Jin, N. R. Gupta, and K. J. Stebe, "The detachment of a viscous drop in a viscous solution in the presence of a soluble surfactant," Phys. Fluids **18**, 022103 (2006).
[30] Y. Cui and N. R. Gupta, "Surfactant effects on drop formation in co-flowing fluid streams," Colloids Surf., A **393**, 111 (2012).
[31] H. A. Stone and L. G. Leal, "The effects of surfactants on drop deformation and breakup," J. Fluid Mech. **220**, 161–186 (1990).
[32] W. J. Milliken, H. A. Stone, and L. G. Leal, "The effect of surfactant on the transient motion of Newtonian drops," Phys. Fluids **5**(1), 69–79 (1993).
[33] E. D. Wilkes, S. D. Phillips, and O. A. Basaran, "Computational and experimental analysis of dynamics of drop formation," Phys. Fluids **11**, 3577–3598 (1999).
[34] B. Ambravaneswaran, E. D. Wilkes, and O. A. Basaran, "Drop formation from a capillary tube: Comparison of one-dimensional and two-dimensional analyses and occurrence of satellite drops," Phys. Fluids **14**, 2606 (2002).
[35] N. R. Gupta, A. Nadim, H. Haj-Hariri, and A. Borhan, "A numerical study of the effect of insoluble surfactants on the stability of a viscous drop translating in a Hele-Shaw cell," J. Colloid Interface Sci. **252**, 236 (2002).
[36] S. Takagi and Y. Matsumoto, "Surfactant effects on bubble motion and bubbly flows," Annu. Rev. Fluid Mech. **43**, 615–636 (2011).
[37] J.-W. Ha and S.-M. Yang, "Effects of surfactant on the deformation and stability of a drop in a viscous fluid in an electric field," J. Colloid Interface Sci. **175**, 369–385 (1995).
[38] J.-W. Ha and S.-M. Yang, "Effect of nonionic surfactant on the deformation and breakup of a drop in an electric field," J. Colloid Interface Sci. **206**, 195–204 (1998).
[39] K. E. Teigen and S. T. Munkejord, "Influence of surfactant on drop deformation in an electric field," Phys. Fluids **22**, 112104 (2010).
[40] Y. Pawar and K. J. Stebe, "Marangoni effects on drop deformation in an extensional flow: The role of surfactant physical chemistry. I. Insoluble surfactants," Phys. Fluids **8**(7), 1738–1751 (1996).
[41] H. A. Stone, "A simple derivation of the time-dependent convective-diffusion equation for surfactant transport along a deforming interface," Phys. Fluids **2**, 111 (1990).
[42] H. Wong, D. Rumschitzki, and C. Maldarelli, "On the surfactant mass balance at a deforming fluid interface," Phys. Fluids **8**(11), 3203–3204 (1996).
[43] C. D. Eggleton, Y. P. Pawar, and K. J. Stebe, "Insoluble surfactants on a drop in an extensional flow: A generalization of the stagnated surface limit to deforming interfaces," J. Fluid Mech. **385**, 79–99 (1999).
[44] S. Velankar, H. Zhou, H. K. Jeon, and C. W. Macosko, "CFD evaluation of drop retraction methods for the measurement of interfacial tension of surfactant-laden drops," J. Colloid Interface Sci. **272**, 172–185 (2004).
[45] I. B. Bazhlekov, P. D. Anderson, and H. E. H. Meijer, "Numerical investigation of the effect of insoluble surfactants on drop deformation and breakup in simple shear flow," J. Colloid Interface Sci. **298**, 369–394 (2006).
[46] C. D. Eggleton, T.-M. Tsai, and K. J. Stebe, "Tip streaming from a drop in the presence of surfactants," Phys. Rev. Lett. **87**, 048302 (2001).
[47] B. Ambravaneswaran and O. A. Basaran, "Effects of insoluble surfactants on the nonlinear deformation and breakup of stretching liquid bridges," Phys. Fluids **11**(5), 997–1015 (1999).
[48] R. V. Craster, O. K. Matar, and D. T. Papageorgiou, "Pinchoff and satellite formation in surfactant covered viscous threads," Phys. Fluids **14**(4), 1364–1376 (2002).
[49] M.-L. E. Timmermans and J. R. Lister, "The effect of surfactant on the stability of a liquid thread," J. Fluid Mech. **459**, 289–306 (2002).
[50] Y.-N. Young, M. R. Booty, M. Siegel, and J. Li, "Influence of surfactant solubility on the deformation and breakup of a bubble or capillary jet in a viscous fluid," Phys. Fluids **21**, 072105 (2009).
[51] P. M. Vlahovska, J. Blawzdziewicz, and M. Loewenberg, "Small-deformation theory for a surfactant-covered drop in linear flows," J. Fluid Mech. **624**, 293–337 (2009).

[52] P. M. Vlahovska, "On the rheology of a dilute emulsion in a uniform electric field," J. Fluid Mech. **670**, 481–503 (2011).
[53] J. Schwalbe, P. M. Vlahovska, and M. Miksis, "Vesicle electrohydrodynamics," Phys. Rev. E **83**, 046309 (2011).
[54] J. Q. Feng and T. C. Scott, "A computational analysis of electrohydrodynamics of a leaky dielectric drop in an electric field," J. Fluid Mech. **311**, 289–326 (1996).
[55] G. Dassios, M. Hadjinicolaou, F. A. Coutelieris, and A. C. Payatakes, "Stokes flow in spheroidal particle-in-cell models with Happel and Kuwabara boundary conditions," Int. J. Eng. Sci. **33**, 1465–1490 (1995).
[56] T. Tsukada, T. Katayama, Y. Ito, and M. Hozawa, "Theoretical and experimental studies of circulations inside and outside a deformed drop under a uniform electric field," J. Chem. Eng. Jpn. **26**, 698 (1993).
[57] O. Vizika and D. A. Saville, "The electrohydrodynamic deformation of drops suspended in liquids in steady and oscillatory electric fields," J. Fluid Mech. **239**, 1–21 (1992).